Coarse-Grained Simulations of Gels of Nonionic Multiblock Copolymers with Hydrophobic Groups

Joshua A. Anderson* and Alex Travesset*

Department of Physics and Astronomy, Iowa State University and Ames Laboratory, Ames, Iowa 50011

Received May 18, 2006

ABSTRACT: Solutions of multiblock nonionic polymers with hydrophobic blocks in water exhibit crystalline and liquid-crystalline phases over a narrow temperature range. This strong temperature sensitivity, critical in the design of novel self-assembled materials, is the result of the drastic increase of hydrophobicity combined with the weakening of solvating interactions (hydrogen bonding or dipolar) as the temperature is raised. In this paper, we separate thermal fluctuations into a "kinetic" temperature and solvation effects and parametrize temperature variations with a single parameter α, where the solvent is modeled implicitly. We provide a microscopic interpretation for this parameter, and molecular dynamics simulations are used to investigate the phases of short ABCBA pentablocks, where the A and C blocks are hydrophobic and the B blocks are hydrophilic but contain hydrophobic groups. At low temperatures and for increasing concentrations, the system undergoes a sol−gel transition. The gel is swollen and consists of highly interconnected spherical micelles with a finite lifetime. At higher temperatures, lamellar and perforated lamellar phases are found for increasing polymer concentrations, while for intermediate concentrations, the system is found in a supercoiled gel. We find good agreement of our results with modified and inverted Pluronic systems and discuss the relevance for other polymers including hydrophobic blocks such as telechelic or peptide-based polymers.

Introduction

The success of self-assembly as a technique to make new materials hinges on our ability to synthesize or recognize the appropriate components, ranging from simple molecules to complex aggregates, and to identify the environmental conditions that must be met for the components to self-assemble into a material exhibiting the specific physical, chemical, and/or biological properties of interest.[1,2] Polymers offer unique properties as components.[3,4] Ionic polymers (polyelectrolytes) are soluble in water and play a critical role in many biological and industrial processes. Nonionic polymers may also be water soluble if they contain functional groups that form sufficiently strong hydrogen bonds with water molecules.

Polymers in solution interact with each other, leading to spatial and/or temporal organizations such as crystals, liquid-crystals, thermoreversible gels, etc. Our current understanding of these organizations and their dependence on chemical composition, chain topology, solvent properties, and other factors is still poor.[5] Multiblock copolymers offer an even wider range of phases and morphologies. Telechelic polymers are ABA triblock polymers, where the B block is a long water-soluble chain and A blocks are short, surfactant-sized hydrophobic chains. Telechelic polymers in solution form flowerlike micelles, which are well understood theoretically[6−8] and are responsible for the relative simplicity of its rheological properties.[9] Pluronic polymers are short (about 100 monomers or less) triblock ABA polymers where A is poly(ethylene oxide) (PEO) and B is polypropylene oxide (PPO) (see ref 10 for a recent review). The phase diagram of Pluronic polymers as a function of temperature, polymer concentration, chain length, and relative fraction of PEO to PPO monomers is fascinatingly diverse and encompasses all phases observed in diblock copolymer melts[9,11] and many others, such as nematic and cubatic liquid-crystalline phases.[9]

* Corresponding authors. E-mail: joaander@ameslab.gov (J.A.A.); trvsst@ameslab.gov (A.T.).

Pluronic and telechelic polymers are just two examples exhibiting the diversity of phases and morphologies of solutions of multiblock polymers that combine both hydrophilic and hydrophobic blocks. The synthesis of novel multiblock copolymers and surfactants that self-assemble into new phases and morphologies has become a very active field. Recent examples include toroidal supramolecular assemblies,[12] Y-junction micelles,[13] and dendritic surfactants showing a number of phases that include an A15 lattice.[14] This A15 lattice is characteristic of a minimal area tiling of the three-dimensional space,[15] and it has recently been predicted[16] to be a stable phase in melts of branched copolymers. Another example of polymer synthesis is the attachment of 2-(diethylamino)ethyl methacrylate (DEAEM) blocks to the ends of a Pluronic F127 polymer.[17] DEAEM blocks are hydrophobic at high pH (pH $\geq$ 8), but as the pH is lowered, the DEAEM groups gain a proton, become charged and, therefore, hydrophilic.[18] The combined Pluronic−DEAEM system (PLD) is both strongly temperature and pH sensitive, where the strong temperature sensitivity is inherited from the Pluronic chain and the pH sensitivity results from the DEAEM end blocks. This rich sensitivity to external changes allows the investigation of self-assembled structures by precisely and independently tuning the relative strength of hydrogen-bonding, electrostatic, and hydrophobic forces.

In this paper, we provide a general model to investigate nonionic multiblock polymers in solution, where one or several blocks contain hydrophobic groups, and present concrete results for the PLD system for which abundant experimental data exists.[17,19,20] Previous MD simulations of the PLD system have been performed with a model where the solvent is considered explicitly.[21] Such simulations are appropriate to explore the structure of single micelles but are still computationally too costly for determining phase diagrams. Implicit solvent models enable simulations of large systems.[22−24] Although several effects may not be reliably accounted for, most notably hydrodynamics, implicit models are expected to provide an accurate description of static equilibrium properties.

10.1021/ma061120f CCC: $33.50
Published on Web 06/27/2006

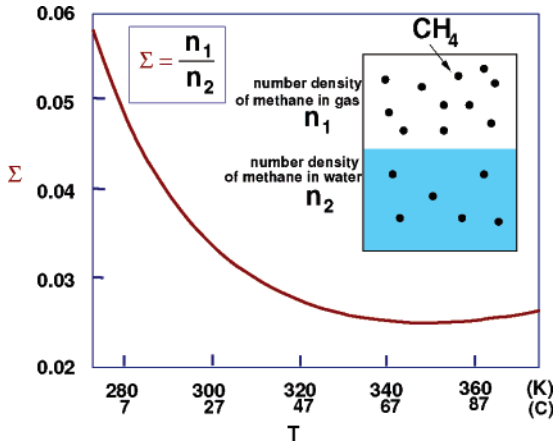

Figure 1. Ostwald coefficient ∑ of methane as a function of temperature (ref 26 and references therein) showing the drastic change in solubility as a function of temperature.

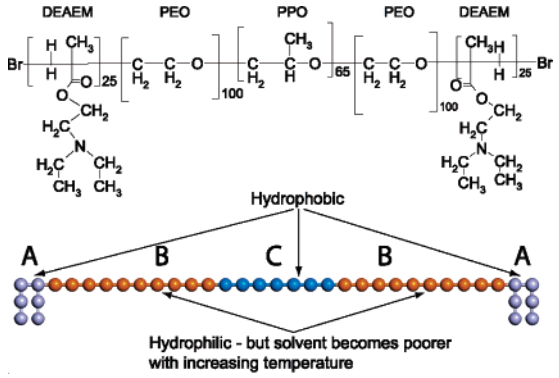

Figure 2. PLD system consists of a F127 pluronic with DEAEM groups attached at both ends (adapted from ref 20). Below, we show the model representation used in the simulations. At high pH, DEAEM are hydrophobic.

Model

Temperature Sensitivity of Hydrophobic Monomers. A common characteristic of soluble polymers containing hydrophobic blocks is their strong temperature sensitivity. In Pluronics, for example, different phases are observed over the narrow temperature range between 10 and 60 °C, with more ordered phases found for *increasing* temperature.[25]

The origin of this anomalous behavior results from the drastic increase in hydrophobicity combined with the weakening of hydrogen-bonding interactions, which enhance solubility, as temperature is increased. The temperature dependence of the hydrophobic effect can be seen in the analysis of the Ostwald coefficient for methane.[26] As shown in Figure 1, an increase in temperature of 35 °C, in absolute temperatures ($\Delta T/T$) ∼ 10%, results in an increases of hydrophobicity by a factor of 2. Longer alkanes follow similar trends,[26] so we assume a similar hydrophobic effect for polymers containing hydrocarbons. In Pluronics polymers, the oxygen in the PEO groups has a strong hydrogen-bonding interaction with water molecules, which is enough to keep PEO soluble at all temperatures.[5] In PPO monomers, however, the additional methyl group (see Figure 2) is enough to drive them insoluble at around 10 °C.

The consequence of Figure 1 is that the quality of the solvent (water) for hydrocarbons is rapidly decreasing over a narrow temperature range. Coarse-grained models for polymers containing hydrocarbon groups where the solvent is modeled implicitly or with a simplified potential must consider potentials with a strong temperature sensitivity. Otherwise, solubility will inevitably increase with temperature.

The phase diagram of an aqueous solution of PEO as a function of temperature and concentration is complex and has been the subject of recent studies.[5,27] In this paper, we consider short PEO blocks at temperatures within the range 10−80 °C. In this region of the phase diagram, PEO blocks are well described as a chain in a good solvent.

Model and Simulation Details. The polymers we consider in this paper are pentablock copolymers with an ABCBA structure. As shown in Figure 2, each A block is composed of 6 beads and has two branches, the B blocks consist of 10 beads, and the C blocks of 7 beads; each polymer contains a total of 39 beads. The choice of 10 Kuhn monomers for block B is consistent with a chain of 100 PEO units as it follows from experiment values.[28] The number of Kuhn monomers of the other blocks are then fixed by mimicking the composition of the real PLD system,[17] as illustrated in Figure 2.

We describe the nonbonding interactions as effective Lennard-Jones 6−12 potentials. Following the discussion at the end of the previous subsection, the beads in both A and C blocks are hydrophobic[1] and interact with a potential

$$U_{\mathrm{AA,AC,CC}}(r) = 4\epsilon\left[\left(\frac{\sigma}{r}\right)^{12} - \left(\frac{\sigma}{r}\right)^{6}\right] \tag{1}$$

PEO monomers are soluble in water, but the quality of the solvent is strongly temperature dependent. This property is modeled by a parameter α (0 ≤ α ≤ 1), with the solvent becoming of poorer quality with an increasing value of α. Thus the interaction of B with all beads is

$$U_{\mathrm{BA,BB,BC}}(r) = 4\epsilon\left[\left(\frac{\sigma}{r}\right)^{12} - \alpha\left(\frac{\sigma}{r}\right)^{6}\right] \tag{2}$$

At α = 0, this potential is purely repulsive

$$U(r) = 4\epsilon\left(\frac{\sigma}{r}\right)^{12} \tag{3}$$

so a given B bead will avoid all other nonbonded beads and prefer contact with the solvent. At α = 1, the interactions of B are the same as with A and C and therefore hydrophobic. It should be noted that a similar model has been recently used to investigate the globular-to-coil transition.[29] All beads in our model have the same mass m and interaction range σ. It has recently been shown[30] that the solvent significantly modifies the packing of the polymer as compared with the same situation without solvent. This effect becomes particularly important for solvents bulkier than water, like benzene, but even in this case, the effect is short-ranged (less than 1 nm), so it is reasonable to expect that it can be incorporated into the parameters of the coarse-grained description.

The hydrophobic effect is the driving force responsible for the different structures observed, and in our model, the hydrophobic interaction is parametrized by α (see eq 2). Within the temperature range between 10 and 45 °C, thermal fluctuations are around $\Delta T/T$ ∼ 10%, while hydrophobic interactions change by a factor of around two, as discussed in the previous section. In our simulations, we will keep the *kinetic* temperature fixed and assume that temperature variations are fully accounted for by the parameter α. From previous considerations, the error involved in this approximation should be of the order of 10%, which is most likely less than the error resulting from coarse-graining and treating the solvent implicitly.

The nearest beads within the polymer chain are connected by a harmonic potential given by

$$U_b(r) = \frac{1}{2} k_b (r - r_0)^2 \tag{4}$$

with $k_b = 330\ \epsilon\sigma^{-2}$ and $r_0 = 0.84\ \sigma$ to avoid bond crossing. The polymers are considered to be completely flexible without any bending potential.

Simulations are carried out with the DL_POLY[31] simulations package. A number N_{poly} of polymers are considered in a finite cube of length L with periodic boundary conditions. The monomeric packing fraction ϕ_P is related to L and N_{poly} by

$$\phi_P = \frac{\pi N_{poly} N_{mon}}{6L^3} \tag{5}$$

where the number $N_{mon} = 39$ is the number of beads per polymer. All potentials are cut off at a value $r_c = 3\ \sigma$. Simulations are performed in the canonical NVT ensemble using the Nose−Hoover thermostat[32] for temperature control. The equations of motion are integrated using the Verlet leapfrog algorithm with a time step $\Delta t = 0.00203\ \tau$, where $\tau = \sqrt{m\sigma^2/\epsilon}$ is the unit of dimensionless time.

The initial configuration is generated using the GenPol package.[33] GenPol uses a combination of Monte Carlo and molecular dynamics algorithms to create relaxed homogeneous polymer chains.

In the simulation runs of the swollen gel phase, the system is equilibrated for 1 million time steps. After the equilibration period, the configuration of the system is recorded every 20 000 time steps as it runs for an additional 4 million. Figure 3 shows the typical behavior of the potential energy and the number of micelles during these runs. The number of micelles is given as a quantity more sensitive to the structure than the potential energy from which equilibration at 1 million time steps is clearly demonstrated. Judging from the micelle lifetimes (see Figure 11 and containing section), a very conservative lower bound of the number of independent configurations for a single simulation run is about three. Considering that each configuration contains ≈200 micelles, that already gives a total of ≈600 independent micelles from which to generate statistics. We recall that, in the micelle lifetime movie (see the Supporting Information), it is clearly seen that micelles change drastically in shape and size in less than half of their lifetime, so the actual number of independent configurations is expected to be significantly larger than three.

The concentrated regime equilibrates *much* more slowly, and these simulation runs are usually equilibrated after 12−15 million time steps. Overall, the total CPU time employed to run the simulations reported in this paper is around 2.2 years on a single 3.2 GHz Intel Xeon processor.

Observable Quantities. The system investigated here generally forms micelles whose structure and superstructure we characterize with various observables. The first step is to identify individual micelles, and we proceed with a similar criteria used previously by other authors:[24,34] Any A or C bead that lies within a distance r_{cut} of any A or C bead belonging to a micelle is included in that micelle. To identify micelles for a fairly large numbers of polymers (N_{poly} of the order 1000), an efficient algorithm is required. Consider the set of A and C monomers to be a fully connected graph. Each bead is a node in the graph, and each edge has a weight equal to the distance between the beads. Then edges longer than r_{cut} are removed. Now, finding the beads belonging to each micelle is equivalent to finding the largest set of spanning trees that cover a partitioning of the graph. This can be done using a bottom-up algorithm with running time $\in\Theta(n^2)$,[35] where n is the number of A and C beads. The identified micelles are insensitive to r_{cut} from 1.22 σ to 2.00 σ. The value $r_{cut} = 1.44\ \sigma$ is used in all results presented in this paper.

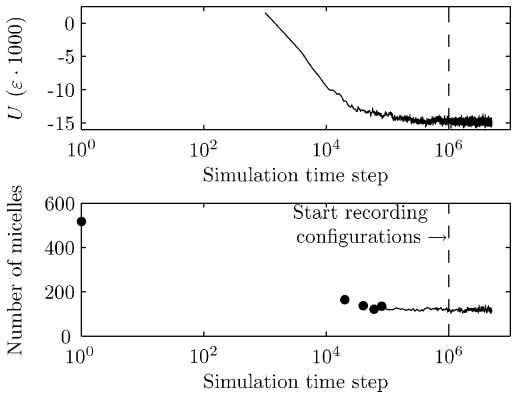

Figure 3. Typical time evolution of the configuration energy and number of micelles during the simulations. Configuration data needed to calculate the number of micelles is only sampled every 20 000 time steps, so markers are drawn for the first few data points.

Let N_{agg} be the aggregation number of a given micelle. With ≈200 micelles forming per configuration, the distribution of N_{agg} is of interest. Let $W(N_{agg})$ be the number of micelles with aggregation number N_{agg} in a given configuration, then the aggregation number distribution is found from

$$w(N_{agg}) = \frac{W(N_{agg})}{\sum_{N_{agg}} W(N_{agg})} \tag{6}$$

The shapes of the micelles are characterized from the gyration tensor[34]

$$G_{\alpha\beta} = \frac{1}{N} \sum_{i=1}^{N} \langle (r_{i,\alpha} - R_{cm,\alpha})(r_{i,\beta} - R_{cm,\beta}) \rangle \tag{7}$$

where the index i runs over all *core* hydrophobic beads within the micelle and $R_{cm,\alpha}$ is the center of mass of the micelle. The three eigenvalues of the matrix **G** (ordered as $g_1 > g_2 > g_3$) characterize the radii of a given micelle.

Several observables are used to characterize the superstructures of micelles. We define a *bridging polymer* as a polymer that has hydrophobic blocks in at least two micelles. The bridging fraction f_B is defined as the number of bridging polymers relative to the total number of polymers. Percolation is also of interest, and we define the gel fraction f_{gel} as the fraction of polymers belonging to the largest group of micelles interconnected by bridging polymers.

We also investigate the statistics of the coordination number N_C of a micelle, defined as the total number of different micelles that a given micelle is connected to via bridging polymers. The distribution of coordination numbers $w_C(N_C)$ is defined in the same way as $w(N_{agg})$.

Ordered structures are analyzed by computing the static structure factor,

$$S(\vec{q}) = \frac{1}{N_{poly} N_{mon}} \sum_{i=1}^{N} \sum_{j=1}^{N} \langle e^{i\vec{q}(\vec{r}_i \cdot \vec{r}_j)} \rangle \tag{8}$$

and by visual inspection of the configurations.

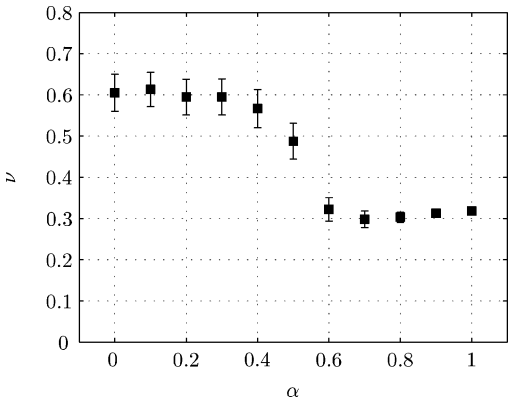

Figure 4. Flory exponent ν as a function of the parameter α for long PEO chains (composed of B beads only). Error bars are displayed at ±1 standard deviation.

Aggregation numbers are variable in time as micelles gain or lose polymers. We thus define the micelle lifetime τ_L as the time taken for a given micelle to lose half of its initial polymers. This is calculated as follows: Let $\mathbf{M}_j^i$ be the set of *core* hydrophobic monomers of micelle j at time step i. For each recorded time step k, the set intersection $\mathbf{I}(j, k, m) = \mathbf{M}_j^0 \cap \mathbf{M}_m^k$ is calculated for all micelles m in time step k (time step 0 refers to the first time step after equilibration). The micelle $m = m_{max}$ that gives the largest number of elements in $\mathbf{I}(j, k, m)$ is identified as the "same" micelle as j. The lifetime τ_L is then defined as the first time step, where the number of elements in $\mathbf{I}(j, \tau_L, m_{max})$ is less than half that in $\mathbf{M}_j^0$.

Solvent distribution is also of interest. In our model, solvent is implicit, so we compute the solvent distribution from the following; Spheres of radius 3 σ are placed on a grid in the simulation box, and local distributions $\phi_{P,X}$ for X = A, B, C beads are calculated inside each sphere. The solvent distribution $\phi_{P,S}$ is then obtained from $\phi_{P,S} + (\phi_{P,A} + \phi_{P,B} + \phi_{P,C}) = c$. The constant c defines the packing fraction and is chosen by assuming that "solvent" beads are absent in regions of high hydrophobicity, where only A and C beads are present. The value $c \approx 0.57$, which corresponds to random loose packing, was consistently used.

Results

The α Parameter and the Assumption of Constant Kinetic Temperature. It is assumed that A and C blocks are hydrophobic and B blocks hydrophilic, but with the solvent becoming of poorer quality for increasing temperature. We provide a more quantitative mapping of the parameter α to the quality of the solvent by simulating a single polymer chain consisting only of B beads and computing the Flory exponent ν (by extrapolating the gyration radius as a function of increasing number of Kuhn lengths) as a function of the parameter α. The results in Figure 4 show a Flory exponent corresponding to a good solvent $\nu \approx {}^3/_5$ in the region with α from 0 to 0.4, a Θ point $\nu \approx {}^1/_2$ around $\alpha \approx 0.45$, and poor solvent $\nu \approx {}^1/_3$ in the region $\alpha \geq 0.45$. In simulations of PLD systems, where the B blocks are PEO and hydrophilic at all temperatures, the values of α are restricted to $\alpha < 0.4$.

We further assume that the dominant effect of the temperature is parametrized by α, while the kinetic temperature is kept fixed. We briefly examine this assumption with the coarse-grained PLD model, shown in Figure 2; $w(N_{agg})$ is calculated at fixed α and ϕ_P and varying values of the kinetic temperature. Generally, large aggregation numbers are entropically unfavorable, and smaller aggregation numbers should be expected for increasing temperature. The results in Figure 5 confirm this tendency and show that thermal fluctuations are not significant as k_BT/ϵ ranges from 1 to 1.2, but they become quite significant at $k_BT/\epsilon = 1.3$, shifting to considerably lower aggregation numbers. We therefore interpret $k_BT/\epsilon = 1.3$ as a critical temperature where thermal effects are dominant over the potential energy and will restrict the temperature within the domain $k_BT/\epsilon < 1.3$. We recall that, if we associate $k_BT/\epsilon = 1$ to a temperature around 10 °C, $k_BT/\epsilon = 1.3$ is a temperature of around 90 °C, so the approximation of constant "kinetic" temperature allows exploration of the relevant temperature range.

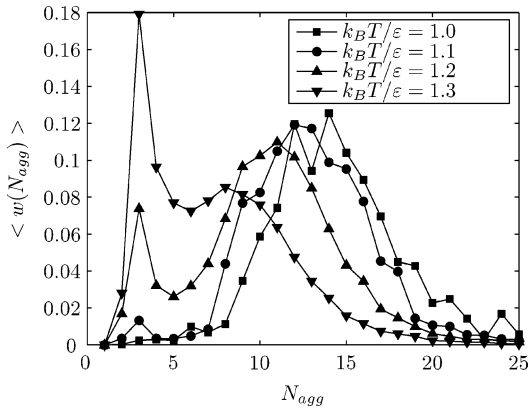

Figure 5. Average micelle aggregation number distribution at α = 0.0, $\phi_P = 0.08$, and at various kinetic temperatures.

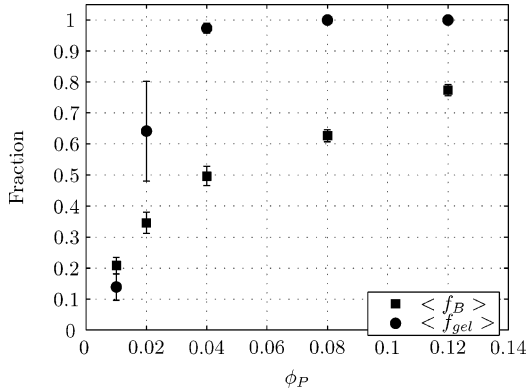

Figure 6. $\langle f_B \rangle$ and $\langle f_{gel} \rangle$ as a function of concentration at α = 0.0. Error bars are displayed at ±1 standard deviation. A sharp transition in both $\langle f_{gel} \rangle$ and $\langle f_B \rangle$ is observed from $\phi_P = 0.02$ to $\phi_P = 0.04$.

The Swollen Gel. If B blocks are strongly hydrophilic, α = 0, micelles consisting of cores of A and C beads and a corona of B blocks are formed. At low polymer concentration ϕ_P, the micelles are spaced far apart and the system consists of almost independent micelles. As ϕ_P is increased, micelles move closer together and become physically connected by bridging polymers. At a critical concentration, all micelles are connected and the system is a gel.

The gelation order parameter is $f_{gel} = 1.0$, indicating that polymers are connected (percolate) through the entire solution.[36] The critical gelation concentration ϕ_P^c (the lowest polymer concentration where $f_{gel} \approx 1.0$) is obtained by inspection of Figure 6 and is $\phi_P^c \approx 0.04$. Examination of the snapshot in Figure 7 corroborates this; the gel is swollen and is composed of roughly spherical micelles. The sol−gel transition is very sharp, as at $\phi_P = 0.02$, the system is deep in the sol phase, while $\phi_P = 0.04$ is already in the gel phase. Also plotted in Figure 6 is f_B, the fraction of polymers bridging different micelles. This number is remarkably high, and for example, at the critical gelation concentration $\phi_P^c \approx 0.4$, only half of the

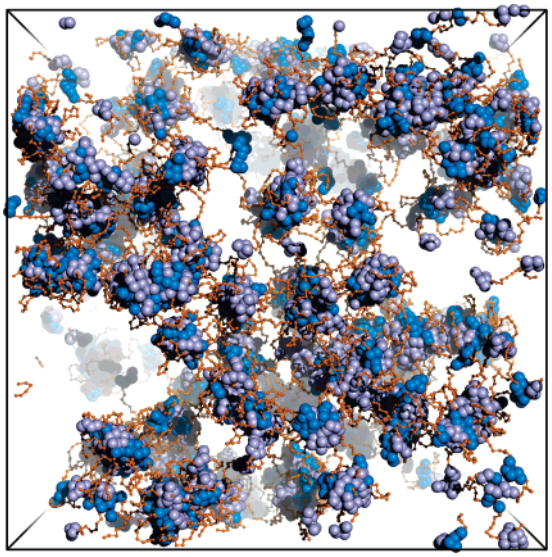

Figure 7. Snapshot of the simulation in the swollen gel phase at $\phi_P = 0.04$. A beads are colored light blue, B orange, and C dark blue. The A and C beads are drawn with a radius of 0.8 σ. B beads are shown smaller so that the view of the micelle core structure is not obscured. Lines also connect the B monomers, showing the bonds between beads in the polymer. Last, the micelles in the background fade out rapidly so that those in the foreground may be seen more clearly. All snapshots are created with PyMOL.[39]

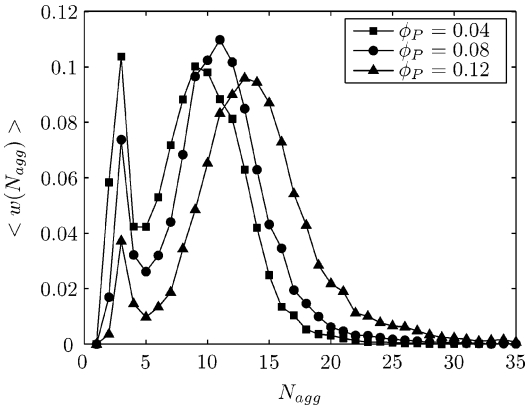

Figure 8. Average micelle aggregation number distribution at $\alpha = 0.0$ for various concentrations.

polymers are fully contained within a single micelle. For higher concentrations, polymers fully contained in a single micelle become increasingly rare. The results in Figures 6 and 7 are indicative of a swollen gel consisting of highly interconnected micelles. These results are qualitatively similar to previous studies in triblock colpolymers.[37]

The average micelle aggregation number distribution is shown in Figure 8 for various concentrations ϕ_P within the range 0.04−0.12. As the concentration is increased, the distribution is shifted slightly to larger aggregation numbers, yet the number density of micelles increases, as shown in Figure 9. Actual micelle number densities are only slightly less than what would be expected if N_{agg} remained constant. This shows the relatively minor effect that concentration has on micelle sizes.

A rough idea of the superstructure of the micelles can be investigated from the average coordination number distribution $w_C(N_C)$, which is shown in Figure 10. N_C has a broad distribution that shifts toward higher values with higher concentration. The position of the peaks and even the shape of the distribution correspond closely with the aggregation number distribution in Figure 8. This is consistent with a given micelle coordinating

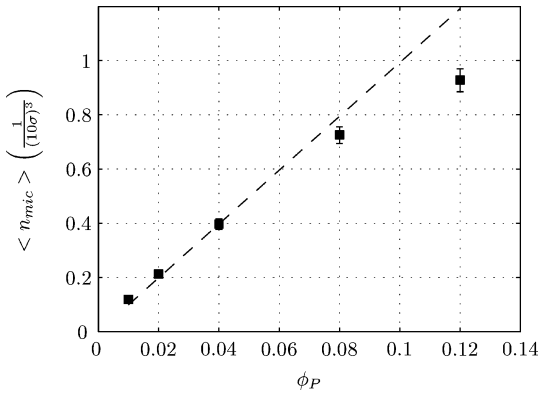

Figure 9. Number density of micelles as a function of concentration at $\alpha = 0$. The dotted line shows what is expected if $\langle N_{agg} \rangle$ at $\phi_P = 0.04$ was to remain constant for all ϕ_P.

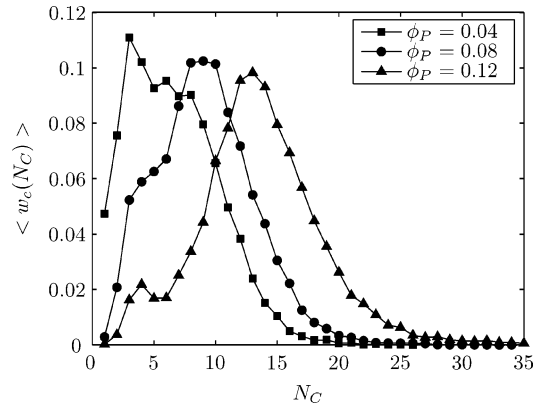

Figure 10. Average distribution of micelle coordination numbers at $\alpha = 0.0$.

with as many other micelles as it has polymers to do so. But $\langle f_B \rangle$ from Figure 6 shows that *not all* of the polymers are bridging. This implies that there are a number of polymers bridging three micelles together with one hydrophobic block in each.

Thermal motion causes micelles to occasionally detach from the percolating gel, and consequently, roughly 4% of the micelles at $\phi_P = 0.04$ actually have $N_C = 0$. This is in agreement with $\langle f_{gel} \rangle$ slightly less than one in Figure 6.

Ratios of the gyration radii provide a quantitative look at the shape of the micelles. For a perfect sphere, all ratios would equal 1.0. As seen in the snapshot (Figure 7), the micelles that form in our system are roughly spherical at $\alpha = 0$. The ratio of the longest radius to the shortest $\langle g_1/g_3 \rangle = 2.2 \pm 0.75$, and the middle to the shortest $\langle g_2/g_3 \rangle = 1.4 \pm 0.23$. Given that these data is calculated from a conservative estimate of ≈600 independent micelles, this spread (one standard deviation) is *not* the result of small statistics; instead, there is a wide variation in micelle shapes. However, all are roughly spherical as long cylinders would be characterized by a larger $\langle g_1/g_3 \rangle$.

Micelle lifetimes are shown in Figure 11 in the range $\phi_P = 0.01-0.12$. The free energy cost of having hydrophobic units in contact with the solvent is high, and therefore it should be expected that isolated micelles are very stable. If other micelles are near, however, a chain can bridge between micelles and eventually transfer from its original micelle to its neighbor by thermal motion. All of these considerations are in agreement with the results in Figure 11, where the micelle lifetime is largest at low concentrations $\phi_P = 0.01$ and decreases with concentration in parallel to the increase in number density of micelles (see Figure 9). Rather interestingly, micelle lifetime shows a plateau at $\phi_P \geq 0.08$. This implies that there is some competing

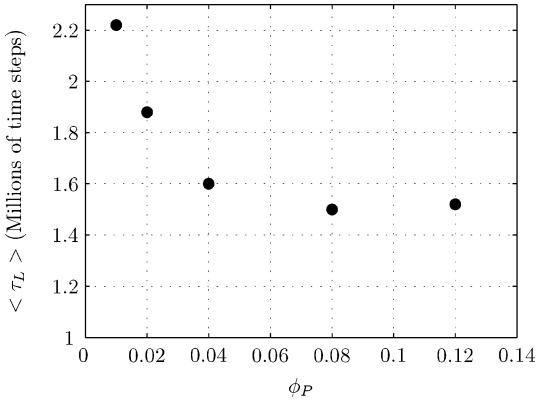

Figure 11. The average micelle lifetime as a function of concentration at $\alpha = 0$.

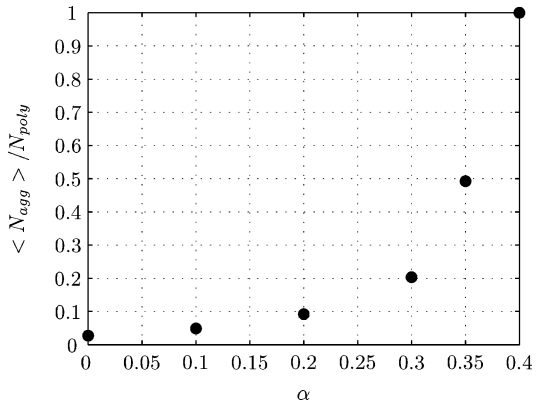

Figure 12. Average aggregation number of micelles for $\phi_P = 0.04$. In these runs, $N_{poly} = 600$.

factor decreasing the rate of polymer transfer. Quantitative comparisons of micelle lifetimes and polymer transfer are strongly dependent on the nature of the solvent and so will not be considered in this paper.

The dynamical nature of the swollen gel is clearly visualized in the movie provided in the Supporting Information. From start to finish, this animation covers 1 million time steps of simulation time with frames spaced 5000 time steps apart. Beads are depicted in the same manner as in Figure 7, except that the polymers belonging to one micelle in the first frame are colored red. Some other polymers are colored green. The evolution of red polymers are observed as a function of time, and the dynamics of the micelle lifetime, including polymer transfer processes, are readily visualized. Creation of micelles are also visualized; the green polymers are initially well separated in space, but as a function of time, they come together and form a new micelle.

The structure factor of the gel, which is provided in the Supporting Information, indicates a liquidlike structure with no evidence for any additional order, either crystalline or liquid crystalline.

The Swollen to Dry Transition. We now investigate the properties of the gel as the B blocks become less hydrophilic by increasing α from 0 to 0.40, following the discussion from Figure 4. As α is increased, micelles are brought closer together as the B beads in the micelle coronas effectively attract one another, resulting in overall larger aggregation numbers and fewer micelles. As shown in Figure 12, the aggregation numbers steadily increase with α. The effect is small at first, but around $\alpha \sim 0.2$, aggregation numbers grow quite rapidly, eventually collapsing all polymers in the simulation box into one giant micelle as α nears 0.40. A plot of micelle number density, shown

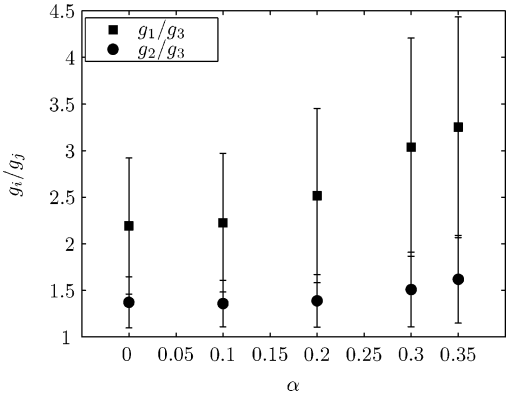

Figure 13. Gyration radii ratios as a function of alpha. Results for $\phi_P = 0.04$ are shown, but there is little difference for ϕ_P from 0.04 to 0.12. Error bars are shown at one standard deviation.

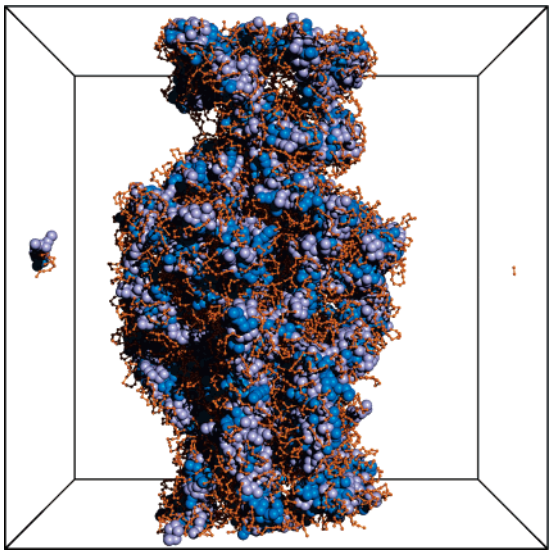

Figure 14. Snapshot of the simulation at $\phi_P = 0.04$ and $\alpha = 0.4$ showing a cylindrical micelle.

in the Supporting Information, confirms the decrease of the number of micelles for increasing values of the α parameter with an almost linear dependence.

The characteristic size of the micelles is very sensitive to α. As α is increased, micelles evolve from a roughly spherical shape to a more cylinder-like one. The ratios g_i/g_j are used to quantify this transition; Figure 13 shows the results. The large variation in shapes seen at $\alpha = 0$ remains for higher α, but the trend for $\langle g_2/g_3 \rangle$ increases dramatically. But even at $\alpha = 0.35$, $\langle g_2/g_3 \rangle$, the ratio of the middle radius to the shortest remains small, implying a roughly circular cross section. These two taken together show relatively long micelles with roughly circular cross sections suggestive of cylindrical micelles.

A snapshot of the system at $\alpha = 0.4$ is shown in Figure 14. Visual inspection indeed shows cylindrical wormlike micelles. Their cores consist of A and C beads, with B beads in the corona. These wormlike micelles bunch together so that many B beads are not even in contact with the solvent. Figure 14 also shows the presence of giant micelles at $\alpha = 0.4$, that is, micelles that wrap around the simulation box. We will further discuss the significance of these micelles in the next section.

Results at slightly higher concentrations $\phi_P = 0.08-0.25$ show similar trends, with a swollen gel phase of roughly spherical micelles for $\alpha \approx 0-0.25$ and giant cylindrical micelles for $\alpha \approx 0.3-0.4$. The analysis of the structure factor $S(\vec{q})$ shows

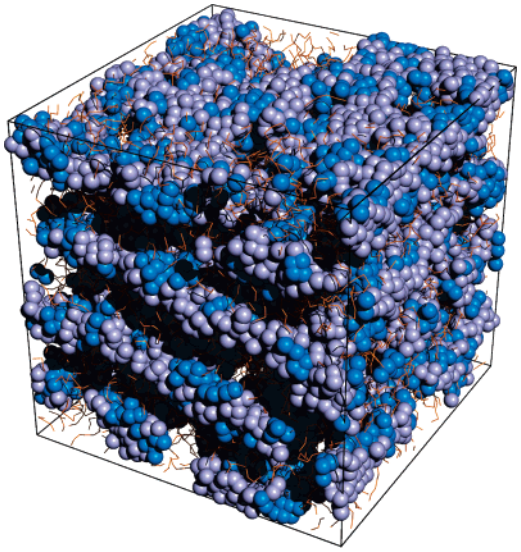

Figure 15. Snapshot of the system at $\phi_P = 0.32$ and $\alpha = 0.35$. Visible perforations are found across the lamellar planes.

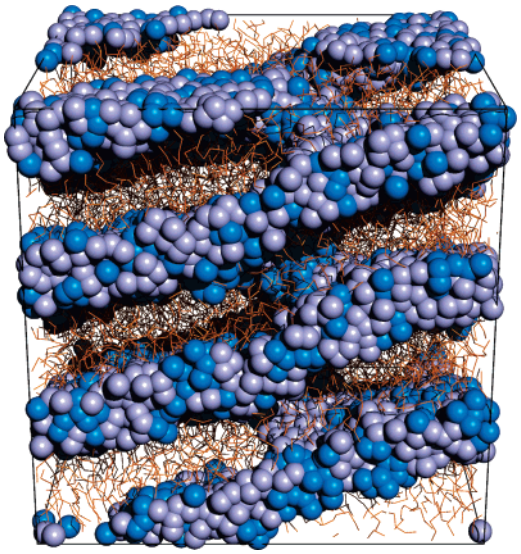

Figure 16. Snapshot of the system for $\phi_P = 0.50$ and $\alpha = 0.35$, forming a lamellar phase. A screw dislocation is clearly visible.

a liquidlike structure for the swollen gel and no particular order within the giant cylindrical micelles.

The Concentrated Regime. The concentrated regime reveals a remarkable degree of order. At polymer concentrations $\phi_P = 0.30$ and $\alpha \sim 0.35$, a perforated lamellar structure is observed in visual inspections of the configurations, as shown in Figure 15. The structure factor $S(\vec{q})$ (shown in the Supporting Information), confirms the lamellar structure. As the concentration is increased, the perforations eventually disappear, leading to a regular lamellar structure. Both regular and perforated lamellar phases are stable against variations of the kinetic temperature $k_BT/\epsilon < 1.3$. If the quality of the solvent is increased, the perforated lamellar phase gradually disappears. In good solvent ($\alpha = 0$), the perforated lamellar is absent and only the lamellar phase is found.

The structure of the lamellar phase consists of planes of A and C beads segregated from the B beads and solvent, which can be seen from the snapshots in Figure 16. A quantitative analysis is shown in Figure 17, where the local distributions $\phi_{P,X}$ of the different beads and solvent are shown. The maximum of the solvent concentration coincides with the maximum of

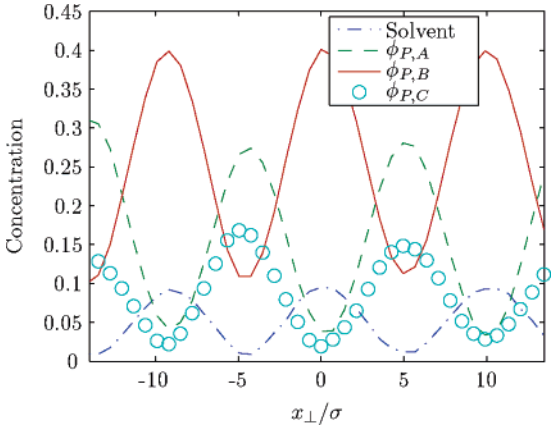

Figure 17. Concentrations of the solvent and A, B, and C beads along the direction perpendicular to the lamellar planes.

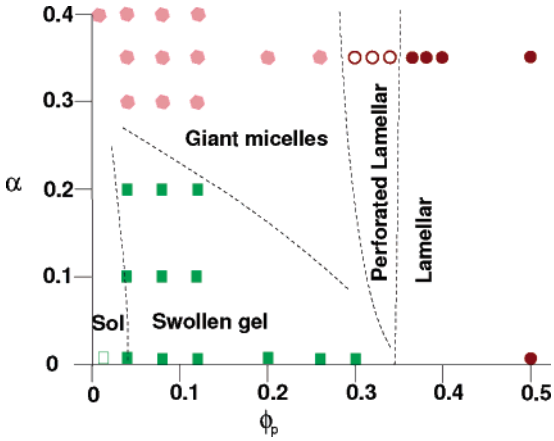

Figure 18. Summary of the results obtained in the previous section. The symbols are points of the phase diagram where actual simulations were run. The boundaries are drawn for a better visualization according to the discussion in the text and are not rigorous.

the hydrophilic B blocks and the minimum of the hydrophobic A and C blocks. This lamellar structure is also corroborated from the analysis of the structure factor shown in the Supporting Information. From the peaks, one extracts a lattice spacing of $\approx 10\ \sigma$, which is in perfect agreement with the thickness of each of the two planes obtained by inspection of the snapshots and from the analysis of the local distributions in Figure 17.

In almost all runs, the regular lamellar phase shows a screw dislocation, which is clearly visible in Figure 16. Only in one run corresponding to $\alpha = 0$, the lamellar phase did not show any topological defects. This may suggest that the elastic constants of the lamellar phase increase with the quality of the solvent.

Discussion

Phase Diagram. The results in the previous section are summarized in Figure 18 and show a sol phase at low concentrations and good solvent for B blocks, followed by a swollen gel and a lamellar phase for increasing concentration. As the solvent for B blocks becomes poorer, a giant micelle that wraps around the simulation box is observed, which is followed by a perforated lamellar and a lamellar phase as the concentration is increased. The points in Figure 18 represent the different simulations presented in parameter space. The perforated lamellar is not found for good solvent $\alpha \approx 0$, as it follows from the results at concentration $\phi_p = 0.3$ and other simulations, which although not fully thermalized (and therefore not shown in the graph), clearly indicated that the system

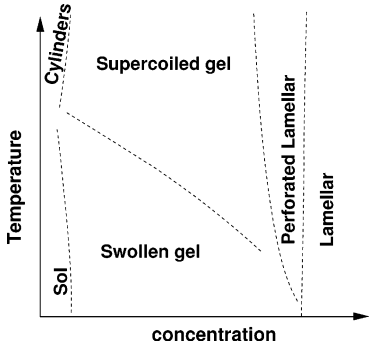

Figure 19. Phase diagram of the PLD system extrapolated from the results in Figure 18. We recall that the temperature and concentrations displayed in the plot are not a linear function of the temperatures and concentrations in the real system.

remained in a swollen gel. We also expect that the critical concentration between the sol−gel transition should decrease with temperature as higher aggregation numbers are more easily formed. For the same reason, we also expect the giant micelles to become possible at lower temperatures for increasing concentration. This discussion is summarized in Figure 18.

The sol, swollen gel, perforated lamellar, and lamellar correspond to phases that should be observed in experiments (a point we discuss further below). The region described as giant micelles, however, corresponds to large micelles wrapping around the simulation box and are therefore a result of the finite simulation box and the periodic boundary conditions used in our simulations. At low concentrations, we interpret the results as implying roughly long wormlike cylindrical micelles. As polymer concentration is increased or solvent quality decreased, we expect these micelles to aggregate, forming increasingly larger and more complex structures. On further increase of either solvent quality or concentration, we expect these aggregates to segregate (precipitate), forming what is known as a supercoiled gel.[38] The supercoiled gel consists of a high polymer concentration with a low water content. For this composition, Figure 18 predicts a lamellar phase. It should be noted, however, that other processes may take place. For example, the supercoiled gel may result from condensation of cylindrical micelles or from aggregation of more disordered structures, with subsequent reorganizations after they precipitate. That is to say, the structure of supercoiled gels is not only dependent on the *final ensemble* but also on the *preparative ensemble*.[38]

The expected phase diagram relevant for experiments is shown in Figure 19. The sol phase is a micellar liquid with some micelles clustering together. This is followed by a swollen phase. Solvent quality is parametrized by α, which is a monotonic function of temperature. So, for increasing temperature, we expect the micelles to grow in size, leading to a liquid of cylindrical wormlike micelles and a supercoiled gel, depending on concentration. The determination of the structure of the supercoiled gel is beyond the scope for this paper. Finally, the lamellar phases are found at larger concentrations. The sol and swollen phase show large density fluctuations that decrease with concentration. Density fluctuations are small for the other phases except possibly at phase boundaries, which lie beyond the scope of this paper.

Comparison with Experiments. Simulations results can be directly compared to PLD systems at high pH (pH > 8), where the DEAEM block (A beads) are hydrophobic. There is abundant experimental data,[17,19,20] which we compare to the theoretical results in this section.

In the dilute limit (2% in weight), SANS experiments at high temperatures (70 °C) show cylindrical micelles,[20] while for lower temperatures (20 °C), spherical micelles are suggested.[17] In more concentrated regimes (20% in weight), a transparent, yet rigid gel phase is observed up to low temperatures (∼7 °C) using tube inversion and rheological measurements.[19] Further increasing of the temperature above 45 °C, a physical hydrogel, which we identify with the supercoiled gel, is formed. The formation of the hydrogel is very slow at these temperatures and proceeds more quickly at a higher temperature (70 °C). The melt state has also been investigated. Structural studies with SANS report evidence for a lamellar phase,[20] although more experimental evidence will be needed. Equilibration times for both the melt state and the hydrogel are very long (of the order of 1 day). All of our numerical simulations are in good agreement with these experimental results.

The structure of the hydrogel, which as stated, we associate with the supercoiled gel in our simulations, reveals a hexagonal lattice of close-packed cylinders with a water content of around 30% in weight.[20] At this water content, our simulations would predict a lamellar phase, but this lamellar phase corresponds to a different preparative ensemble. We speculate that the hexagonal structure is the result of two steps, the formation of cylindrical micelles and the posterior self-assembly of these micelles into a hexagonal structure. Further work will be needed to clarify this point.

Inverted Pluronics are triblock PPO−PEO−PPO polymers. On a qualitative level, they present some similarities with PLD systems in that they contain hydrophobic end blocks between overall hydrophilic blocks (PEO) and therefore show the same temperature sensitivity discussed for PLD systems. Phase diagrams for these systems have been reported and are qualitatively very similar to Figure 19. The observed phases are a random network (sol phase), a micellar network (swollen gel), and a uniform micellar phase, which we attribute to the supercoiled gel. At higher concentrations, a lamellar phase[40] is also found. Furthermore, these phases follow the same sequence as a function of both concentration and temperature as the one in Figure 19. Many details regarding the boundaries and the critical concentrations separating these phases are quantitatively different, but we regard these results as providing additional evidence on the validity of our theoretical results.

Conclusions

In this paper, we separated thermal effects into a "kinetic temperature" and solvation effects (hydrophobic, and to a lesser extent, hydrogen-bonding), which has allowed parametrizing of the temperature by a single parameter (the α parameter) in an implicit solvent coarse-grained model. We determined the phase diagram of the PLD system both as a function of temperature and concentration and found a swollen and dry gel as well as lamellar and perforated lamellar phases. The results are in good agreement with experimental results on PLD systems and on inverted Pluronics. We provided a cross-check for the validity of our assumptions (Figure 5) and showed that the parameter α is a monotonic function of the temperature, which is well correlated with the Ostwald coefficient for alkanes (Figure 1), which is a measure of the hydrophobic effect. We also provided a detailed characterization of the different phases involved. The model presented is general and is suitable to determine phase diagrams as a function of concentration and temperature for other systems such as Pluronic, telechelic, or peptide-based and other nonionic polymers that are soluble yet contain hydrophobic groups that decrease the solubility of the polymer for increasing temperature.

Explicit solvent models provide a realistic description of the dynamics and a more accurate description of the statics,[21,41−43]

but the CPU cost involved for simulating the large systems ($N_{poly} = 600$) investigated here would be very demanding. From the extensive experience gained in simpler models,[36,38,44] we expect that the main conclusions of this paper will not be modified by the use of an explicit solvent. The system studied in this paper has some connections with the HP copolymers studied recently by scaling methods.[45] We point out, however, that Pluronic and related polymers are short (of the order of 10 Kuhn lengths or less) and scaling theories may not provide an accurate description for these systems.

There are many situations that we expect to discuss further in the future. The polymers investigated in this paper are slightly branched (the A blocks).[46] Recent results in melts show the existence of exotic phases for branched polymers.[16] It is our expectation that polymers with different branching degrees will include the phases found in melts, but by tuning temperature, pH, or concentration, additional phases will be found. The precise control and understanding of these phases provide exciting components for novel thermosensitive self-assembled materials. We hope that the simulations presented in this paper will stimulate further experimental work in this very exciting and relatively unexplored area.

Supporting Information Available: In addition to figures and movies mentioned in the body of this paper, there are DIVX AVI clips of the snapshots. These rotate and/or rock the image to provide a better look at the structures. This material is available free of charge via the Internet at http://pubs.acs.org.

Acknowledgment. We acknowledge many discussions with S. Chushak, M. Determan, C. Lorenz, S. Mallapragada, T. Prozorov, W. Bu, and D. Vaknin. We also thank C. Zaruba for technical assistance. This work has been supported by a DOE grant under contract W-7405-ENG-82 and partially supported by a NSF grant DMR-0426597.

References and Notes

(1) Whitesides, G. M.; Boncheva, M. *Proc. Nat. Acad. Sci. U.S.A.*, **2002**, *99*, 4769.
(2) Kamien, R. *Science* **2003**, *299*, 1671.
(3) Muthukumar, M.; Ober, C. K.; Thomas, E. L. *Science* **1997**, *277*, 1225.
(4) Bucknall, D.G.; Anderson, H. L. *Science* **2003**, *302*, 1904.
(5) Tanaka, F. *Polym. J.* **2002**, *34*, 479.
(6) Semenov, A. N.; Joanny, J. F.; Khokhlov, A. R. *Macromolecules* **1995**, *28*, 1066.
(7) Tanaka, F. *J. Non-Cryst. Solids* **2002**, *307*−*310*, 688.
(8) Sung, B. J.; Yethiraj, A. *J. Chem. Phys.* **2003**, *119*, 6917.
(9) Alexandridis, P; Lindman, B. *Amphiphilic Block Copolymers*; Elsevier: Amsterdam, 2000.
(10) Kabanov, A. V.; Batrakova, E. V.; Alakhov, V. Y. *J. Controlled Release* **2002**, *28*, 189.
(11) Matsen M. W. *J. Phys: Condens. Matter* **2002**, *14*, R21.
(12) Pochan, D. J.; Chen, Z.; Cui, H.; Hales, K.; Qi, K.; Wooley, K. L. *Science*, **2004**, *306*, 94.
(13) Jain, S.; Bates, F. S. *Science* **2003**, 460.
(14) Cho, B.K.; Jain, A.; Gruner S. M.; Wiesner U. *Science* **2004**, *305*, 1598.
(15) Ziherl, P.; Kamien, R. D. *J. Phys. Chem B* **2001**, *105*, 10147.
(16) Grason G. M.; DiDonna B. A.; Kamien R. D. *Phys. Rev. Lett.* **2003**, *91*, 58304.
(17) Anderson, B. C.; Cox, S. M.; Bloom P. D.; Sheares V. V.; Mallapragada S. K., *Macromolecules* **2003**, *36*, 1670.
(18) Asayama, S.; Maruyama A.; Cho, C. S.; Akaike, T. *Bioconjugate Chem.* **1997**, *8*, 833.
(19) Determan, M. D.; Cox, J. P.; Thyagarajan, P.; Mallapragada S. K. *Polymer* **2005**, *46*, 6933.
(20) Determan, M. D.; Guo, L.; Thyagarajan, P.; Mallapragada S. K. *Langmuir* **2006**, *22*, 1469.
(21) Chushak Y.; Travesset A. *J. Chem. Phys.* **2005**, *123*, 234905.
(22) Khalatur, P. G.; Khokhlov A. R.; Mologin D. A. *J. Chem. Phys.* **1998**, *109*, 9602.
(23) Bedrov, D.; Smith, G. D.; Douglas J. F. *Europhys. Lett.* **2002**, *59*, 384.
(24) Guo, L.; Luijten, E. *J. Polym. Sci. B* **2005** *43*, 959.
(25) Wanka, G.; Hoffmann, H.; Ulbricht, W. *Macromolecules* **1994**, *27*, 4145.
(26) Widom, B.; Bhimalapuran, P.; Koga, K. *Phys. Chem. Chem. Phys.* **2003**, *5*, 3085.
(27) Dormidontova, E. E. *Macromolecules* **2002**, *35*, 987.
(28) Flory, P. *Statistical Mechanics of Chain Molecules*; John Wiley & Sons: New York, 1969.
(29) Polson, J. M.; Moore, N. E. *J. Chem. Phys.* **2005**, *122*, 24905.
(30) Mendez, S.; Curro, J. *Macromolecules* **2004**, *37*, 1980.
(31) DL_POLY is a package of molecular simulation routines written by W. Smith and T. R. Forester, copyright The Council for the Central Laboratory of the Research Councils, Daresbury Laboratory at Daresbury, Nr. Warrington, UK, 1996.
(32) Allen, M.; Tildesley, D. *Computer Simulation of Liquids*; Clarendon Press: Oxford, 1987.
(33) Kroger, M. *Comput. Phys. Commun.*, **1999**, *118*, 278.
(34) Maiti, P. K.; Lansac, Y.; Glaser, M. A.; Clark, N. A.; Rouault, Y. *Langmuir* **2002**, *18*, 1908.
(35) Brassard, G.; Bratley, P. *Fundamentals of Algorithmics*; Prentice Hall: New York, 1996.
(36) Rubinstein, M.; Colby, R. *Polymer Physics*; Oxford University Press: New York, 2003.
(37) Halperin, A.; Zhulina, E. B. *Europhys. Lett.* **1991**, *16*, 337.
(38) De Gennes, P. G. *Scaling Concepts in Polymer Physics*; Cornell University Press: Ithaca, NY, 1979.
(39) DeLano, W. L. *The PyMOL Molecular Graphics System*; DeLano Scientific: San Carlos, CA, 2002; http://www.pymol.org.
(40) Mortensen, K.; Brown, W.; Jorgensen, E. *Macromolecules* **1994**, *27*, 5654.
(41) Srinivas, G.; Discher, D.; Klein, M. *Nat. Mater.* **2004**, *3*, 638.
(42) Shelley, J. C.; Shelley, M. Y.; Reeder, R. C.; Bandyopadhyay, S.; Klein, M. *J. Phys. Chem. B* **2001**, *105*, 4464.
(43) Fukunaga, H.; Doi, M. *J. Chem. Phys.* **2002**, *116*, 8183.
(44) Grosberg, A. Y.; Khokhlov, A. R. *Statistical Physics of Macromolecules*; AIP Press: Woodbury, NY, 1994.
(45) Khokhlov, A. R.; Semenov, A. N.; Subbotin, A. V. *Europhys. J. E* **2005**, *17*, 283.
(46) The temperature dependence for these blocks as described by Figure 1 is unnecessary as it is assumed that they are already dehydrated, that is, they avoid the solvent.

MA061120F